IEEE Access
Multidisciplinary | Rapid Review | Open Access Journal

Received April 4, 2020, accepted April 15, 2020, date of publication April 21, 2020, date of current version May 14, 2020.

Digital Object Identifier 10.1109/ACCESS.2020.2989280

Wireless Geophone Sensing System for Real-Time Seismic Data Acquisition

HUSSEIN ATTIA, (Member, IEEE), SAGIRU GAYA, ABDULLAH ALAMOUDI, FAHAD M. ALSHEHRI, ABDULRAHMAN AL-SUHAIMI, NAWAF ALSULAIM, AHMAD M. AL NASER, MOHAMAD AGHYAD JAMAL EDDIN, ABDULLAH M. ALQAHTANI, JHONATHAN PRIETO ROJAS, (Member, IEEE), SUHAIL AL-DHARRAB, (Senior Member, IEEE), AND FERAS AL-DIRINI, (Member, IEEE)

Electrical Engineering Department, King Fahd University of Petroleum and Minerals (KFUPM), Dhahran 31261, Saudi Arabia

Corresponding author: Feras Al-Dirini (feras.aldirini@kfupm.edu.sa)

This work was supported by the Center for Energy and Geo-Processing (CeGP) at King Fahd University of Petroleum and Minerals (KFUPM), Dhahran, Saudi Arabia, under grant number GTEC1802.

ABSTRACT Active seismic surveys, for the exploration of oil and gas reservoirs, are conducted using a huge network of geophone sensors (>10,000) covering a very large area and interconnected using seismic cables. Such cables enable reliable operation and fast data transfer, but account for a major percentage of the survey cost and limit its flexibility. In this paper, a wireless seismic data acquisition system that provides real-time data transmission for active seismic surveys is designed and implemented. A system that comprises a smart wireless sensor node and a gateway unit is demonstrated as a proof-of-concept. The smart wireless node comprises a geophone sensor, a high-resolution data acquisition system and a smart reconfigurable wireless communication module. The data acquisition system includes an electronic circuit for amplification and filtering, a single-board computer and a 24-bit analog-to-digital converter (ADC). The wireless communication module comprises a 2.4 GHz radio frequency (RF) transceiver connected to a pattern reconfigurable antenna. A microcontroller is employed to reconfigure the Yagi-Uda antenna to scan its radiation pattern in different directions and focus the radiated power in the direction of the nearest gateway. This high-gain directional antenna would allow communication between the sensor node and the gateway over a longer distance as compared with the monopole antenna conventionally employed in commercial wireless seismic systems. The proposed system, employing a reconfigurable antenna in the sensor node, has been implemented and tested and was able to successfully capture seismic data from the geophone sensor and transmit it wirelessly in real-time to the gateway unit, achieving a notable 25% enhancement in the communication range between the sensor node and the gateway. This communication range enhancement results in a significant 56% enhancement in the gateway's communication area coverage, when compared to similar systems that use conventional monopole antennas in their sensor nodes.

INDEX TERMS Geophone, seismic acquisition, gateway, wireless node, reconfigurable antenna.

I. INTRODUCTION

Over the past few decades, major industries have been directing their interest and resources towards monitoring and exploration of the Earth's subsurface including its underlying structure and stratigraphy [1]–[10]. Most notably, oil and gas industries have increased their investments in seismic exploration in quest of new oil and gas reservoirs and in pursuit of enabling more efficient production [8], [11], [12].

In seismic surveys, as depicted in Fig. 1, vibration sources on the surface (e.g. vibroseis trucks) generate low frequency vibrations (seismic waves) that propagate through the subsurface layers and geological structures, which in turn attenuate, reflect, and refract these waves [13]. Geophone sensors placed at the surface, usually in an array configuration that covers the whole area under exploration, are then used to detect the reflected components of these seismic waves. Upon proper processing of the collected data from a large number of geophones (usually in excess of 10,000 geophones), high quality seismic images/maps of the Earth's subsurface can

The associate editor coordinating the review of this manuscript and approving it for publication was Emanuele Lattanzi.

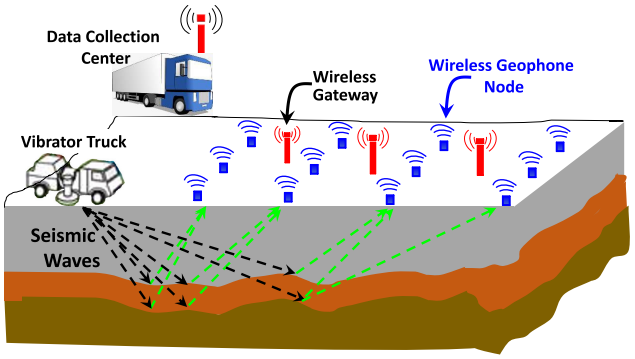

FIGURE 1. The proposed wireless seismic data acquisition system incorporating wireless geophone nodes that communicate with local gateways, which in turn communicate with a central data collection center.

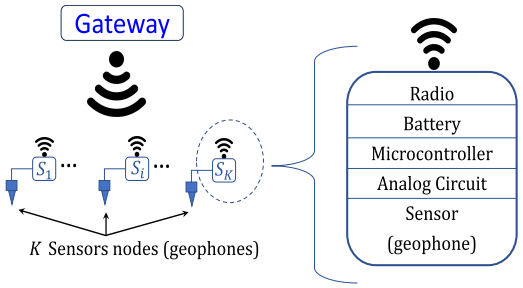

FIGURE 2. A schematic diagram illustrating the concept of a wireless sensor network (WSN) (left), and the components of an individual sensor node (right).

be obtained. These images are then used by geophysical interpreters in identifying certain structures that indicate potential hydrocarbon traps [14].

Traditionally, expensive high-end cables have been used to connect the large number of geophone sensors to the data collection centers, in order to provide the sensors with power for operation and with a communication means for data transmission. Although cabled systems provide reliable uninterrupted operation and high resolution seismic data transfer, their deployment and maintenance costs increase substantially as surveys become massive in scale and density [8]. Furthermore, the complex environment in certain survey areas makes cabled systems expensive and impractical. As a result, there is an inevitable trend in next generations high-density acquisition systems towards flexible platforms that use wireless technologies [3].

The tendency towards wireless acquisition systems has motivated many researchers [2]–[10] and companies [11], [12] to endorse wireless seismic acquisition methods based on Wireless Sensor Network (WSN) architectures, such as the proposed architecture illustrated in Fig. 1. Crice *et al.* in [3] covered the approaches and designs for near-surface seismic acquisition and highlighted the transition in the industry from cabled to cable-less seismic acquisition systems. More recently, Song *et al.* in [15] discussed the big picture of distributed sensor networks for subsurface imaging, describing a framework and an architecture towards the realization of an envisioned *subsurface camera*.

A generic WSN, shown in Fig. 2, consists of K sensor nodes, where each node contains a geophone that detects reflected seismic waves and sends its data to a central local node referred to as the gateway. Usually the acquisition constraints are more stringent on the sensor node side than the gateway, due to the scattered remote deployment of the sensor nodes, which also directly translates to scarcity of power. Although the geophone sensors themselves are passive in operation, each sensor node has, in addition to its geophone sensor, analog circuitry for filtering and amplification of the detected signal, an Analog-to-Digital Converter (ADC) with a micro-computer for digitization and pre-processing of the data, and a Radio Frequency (RF) front-end for communication of the collected digitized data, all of which consume significant amounts of power. Accordingly, this work focuses on the design and implementation of the geophone sensor node (GSN) given these stringent power consumption constraints, with greater focus on optimizing power usage in sending data over the RF link to the gateway.

Nonetheless, it is worth noting that there are several other network designs adopting the WSN concept for seismic acquisition applications focusing on other aspects of the system, such as the network architecture, the technology used for sensing, and the ADC bit resolution [4]–[9]. Moreover, there has been significant recent progress on the design and implementation of WSNs for passive seismic monitoring [16]–[18], which are smaller scale networks - compared to those deployed for active seismic surveys - targeted at a range of different applications, including volcano monitoring.

In this work, a smart wireless geophone sensor network for real-time seismic data acquisition is designed, implemented, and tested. A smart sensor node and a gateway are employed to prove the design concept and its capabilities. The sensor node transmits its data to the gateway through a smart RF front-end equipped with a smart reconfigurable antenna, designed using the Yagi-Uda approach. The antenna operates over the frequency band of 2.35-2.45 MHz, governed by the IEEE 802.15.4 ZigBee standard, with data rates up to 250 kb/s, and is driven by a commercial XBee RF module [19].

Unlike available commercial wireless seismic data acquisition systems [11], [12], that employ conventional low-gain omni-directional wire antennas, the use of the novel high-gain directional antenna system proposed in this work enables the RF front-end to steer its radiated beam towards the nearest gateway for efficient energy focusing and enhanced achieved transmission ranges [20]–[23], as will be demonstrated throughout this paper.

The paper is organized as follows. Section II gives an overview of the complete system design of the proof-of-concept sensor network and its modes operation. In Section III, the high-resolution data acquisition system interfaced with the geophone sensor is presented. Section IV covers the design of the smart RF front-end communication system. Integration, validation, and testing of the proposed

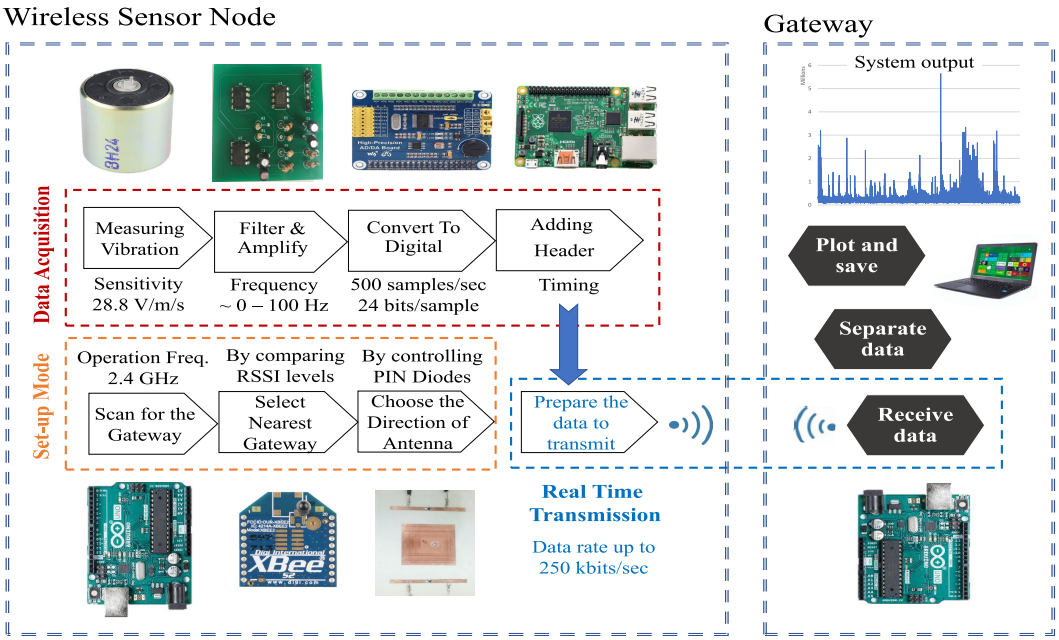

FIGURE 3. Complete block diagram of the proposed wireless geophone sensor network for seismic data acquisition.

system is presented in Section V. The paper is concluded in Section VI.

II. OVERALL SYSTEM DESIGN AND OPERATION

The designed proof-of-concept system includes a wireless Geophone Sensor Node (GSN) and a gateway unit as depicted in Fig. 3. The GSN comprises two main modules, the *data acquisition module* and the *communications module*. The first captures, filters, and amplifies the analog signal received from the geophone sensor, then converts it to digital form, while the latter sends the digital data to the gateway utilizing a smart reconfigurable antenna. Fig. 3 shows the sequence of operations and the flow of data in the proposed system from the time the geophone sensor captures it until it is received at the gateway in digital form.

When the wireless GSN is first installed in the field, seismic waves detected by the geophone get converted into an analog voltage signal. This signal is then filtered and amplified, in order to remove unwanted signal components due to background vibrations and other noise sources. The analog signal is then digitally sampled with a sampling rate of 500 samples per second (SPS) at a resolution of 24 bits per sample by the ADC module. The digital data is then processed in the single-board computer by adding a header to it that includes the timing at which each sample was taken. This data is then saved to the on-board memory within the single-board computer and then passed on to the communication module for real-time transmission to the gateway.

The GSN has been designed to operate in two different modes; *blind* seismic data capturing and *real-time* seismic data monitoring, both of which are discussed herein. If the communication module had previously set-up and established a communication link with a gateway, it will directly send the data in *real-time* to the gateway, operating in real-time seismic data monitoring mode. Otherwise, if no communication link had been previously established, the data acquisition module will continue to capture data and save it to the on-board memory within the geophone node (i.e., *blind* mode), and this data may later on be retained at the end of the data collection cycle from the memory card directly. The design and detailed operation of the data acquisition module and the communications module are discussed in-depth in Sections III and IV, respectively.

III. THE DATA ACQUISITION MODULE

In seismic surveys, employed in oil and gas exploration, the data of interest that needs to be collected by the geophone sensors is the mapping in space and time of the reflected waves. Such reflected waves would have the same frequency of the waves sent by the vibration source, which are usually in the range of 10 - 100 Hz, in order to have long enough wavelengths that allow deep penetration into the earth's sub-layers. Vibrations detected by the geophone at other frequencies may be due to other environmental sources that are of no interest for active seismic surveys, and hence need to be filtered out before any amplification. Based on the above, and as shown in Fig. 4, the data acquisition module of the system would be comprised of three main components; the geophone sensor, electronic circuits for filtering and amplification and an analog-to-digital converter for sampling and digitization of the measured seismic signals. The main source of power for all blocks of the GSN is a solar power bank as shown in Fig. 4. The only exception to this is the Analog circuit, which needs a dual supply that cannot be provided by the solar power bank and hence is powered using two 9 V batteries that can power the Analog circuit for more than a month.

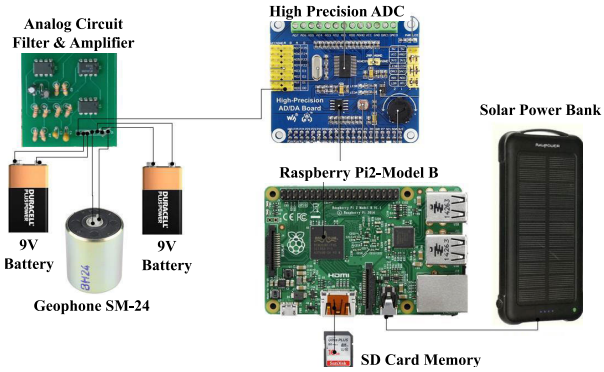

FIGURE 4. The data acquisition module of the geophone sensor node (GSN) for seismic data acquisition.

Each of the three main system components mentioned above is discussed in details in the upcoming three subsections.

A. THE GEOPHONE SENSOR - CAPTURING RAW SEISMIC DATA

A geophone is a ground motion sensor used to convert ground vibrations into voltage. The output voltage represents the deviation in the ground's motion, which forms the raw data that is subsequently processed in order to study the Earth's subsurface. There are several commercially available geophone sensors, each with its unique set of features. In the presented design, an SM-24 [24] geophone model is employed, which offers an extended bandwidth that allows the realization of high resolution recording systems with 2 *m*sec sampling intervals and a resolution of 24 bits per sample. Sampling each 2 *m*sec gives rise to a sampling rate of 500 samples/second and a bandwidth covering the frequency range of interest used in active seismic surveys (10 - 100 Hz). It is important to note that the sensitivity of the used geophone is 28.8 V/m/s.

B. THE ANALOG CIRCUIT - FILTERING AND AMPLIFICATION

The analog circuit, which is shown in Fig. 5, consists of three blocks; a low-pass filter (LPF) followed by an amplifier and then followed by another LPF. The first LPF is used to filter any frequencies detected by the geophone sensor that are outside the frequency range of interest, and hence it has been designed with a theoretical ideal cutoff frequency of around 150 Hz. The amplifier provides the high voltage gain needed for preparing the data to be sampled at high resolution by the ADC. The final filtering stage filters out any noise introduced by the amplification process at higher frequencies and ensures a smoother decay for the low-pass response of the overall circuit. Resistors R_1, R_2, R_3 and R_4, capacitors C_1 and C_2 and $OpAmp_1$ constitute the first second-order active LPF, which has been designed to have an ideal theoretical cut-off frequency of 150 Hz. The low-pass cut-off frequency of the circuit is dependent on its RC time constant according to the following relationship:

$$f_c = \frac{1}{2\pi\sqrt{(R_1R_2C_1C_2)}} = 154Hz \tag{1}$$

where we have selected $R_1 = R_2 = 4.7\ k\Omega$ and $C_1 = C_2 = 220\ nF$. Moreover, since most of the gain will come from

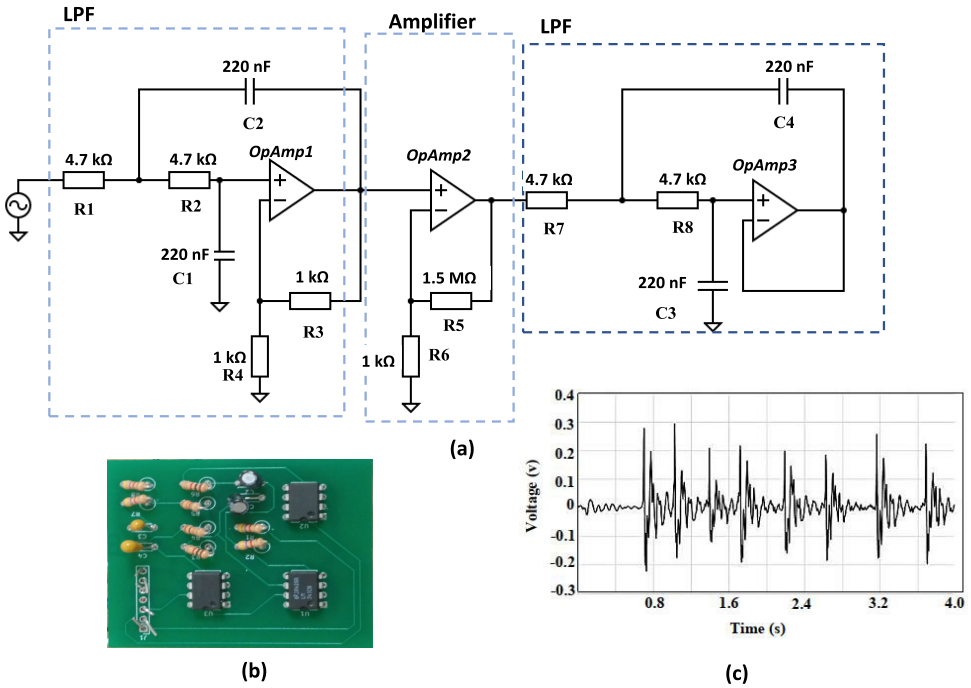

FIGURE 5. (a) A schematic diagram of the designed analog circuit that includes two stages of low-pass filters and an amplifier. (b) Photograph of the implemented circuit mounted on a PCB. (c) A sample plot of the output voltage from the analog circuit in (a). (see Video 1 in the multimedia supplementary materials appended to this article).

the following stage, R_3 and R_4 were selected to be both 1 kΩ giving rise to a small gain of only 2 V/V, according to the following expression

$$A_V = 1 + \frac{R_3}{R_4} \tag{2}$$

The second and most important stage of the analog circuit is composed of resistors R_5 and R_6 along with $OpAmp_2$, as shown in Fig. 5. This stage constitutes the main amplification stage of the circuit. The circuit has been configured in a non-inverting OpAmp configuration, and the gain of this circuit also follows the relationship of (2).

The overall gain of the circuit is mainly achieved through the gain of this stage (i.e., $OpAmp_2$), and this gain needs to be designed based on two factors; the maximum expected voltage generated by the geophone and the maximum voltage that the ADC can support (5 V in our case). The maximum voltage generated by the geophone is expected to be around 1.44 mV, and this can be calculated using the geophone's sensitivity (V/m/s) and the expected maximum speed (m/s) of the reflected waves. It is important to note that the geophone is capable of generating greater voltage amplitudes. However, the above-specified voltage amplitude range applies for seismic signals in active Earth exploration surveys. Such types of surveys are usually conducted in remote areas away from cities and metropolitan areas, such as in deserts, and hence background vibrations and movements are minimal and would result in generating very small voltage amplitudes in the geophone, much below the voltages due to the active seismic waves generated by the vibroseis trucks.

Based on the above explanation, and for our system requirements, the maximum overall voltage gain would be given by

$$G_V = \frac{5\ V}{1.44\ mV} = 3472\ V/V \tag{3}$$

Since the first LPF has a gain of 2 V/V, we designed our second stage to have a gain of 1500 V/V (Therefore $R_5 = 1.5\,M\Omega$ and $R_6 = 1\ k\Omega$). Finally, resistors R_7 and R_8, capacitors C_3 and C_4 and $OpAmp_3$ constitute the second second-order active LPF, without any additional gain and with the same cutoff frequency of around 150 Hz.

The overall gain is then expected to be 3000 V/V or 69.5 dB. After implementing the circuit on a PCB as shown in Fig. 5(b), it was difficult to test the performance of our circuit in a lab bench setup due to constrains in the minimum signal level that can be generated by our function generator, and when trying to use it in a field test within our institution's premise, we realized that due to the very high gain of the system, the background vibrations due to building vibrations and vibrations due to large machinery such as air conditioning systems always resulted in a saturated output reaching the maximum supply voltage. Such sources of vibration would not usually be present in common survey sites away from metropolitan areas, such as in deserts. Based on the above, it was necessary to adjust the overall system gain for testing purposes.

The overall system gain was adjusted by replacing resistor R_4 with a 10 $k\Omega$ resistor and replacing R_5 with a 180 $k\Omega$ resistor, giving rise to a predicted voltage gain of 198 V/V. Fig. 5(c) shows a sample output signal of the analog circuit after filtering and amplification, any vibration would result in a peak with a positive voltage and a trough with a negative voltage. Since our employed ADC is capable of sampling positive voltages only, our system will focus on capturing the peaks. Nonetheless, it would be very desirable to capture the troughs too in future generations of the system, as these troughs can provide useful information that can be used in the interpretation of the data. In order to achieve this, a DC offset needs to be applied to the analog voltage signal, after filtering and amplification but before sampling, in order to move the peaks as well as the troughs to be in the positive voltage range of the ADC. In the multimedia supplementary materials appended to this article, Video 1 shows the experimental lab bench test setup and the waveform extracted from the geophone after amplification and filtering.

Fig. 6 shows the measured and simulated gain of the implemented circuit shown in Fig. 5. A fair agreement between the simulated gain, calculated using LT Spice software, and the measured gain is achieved. A maximum simulated gain of 46 dB is predicted. As can be observed, common losses and tolerances in the values of the used resistors led to a slightly smaller measured overall gain of 44.5 dB, while the parasitic capacitance introduced by the discrete components and circuit connections reduced the overall cut-off frequency to around 100 Hz, satisfying the design requirement of capturing seismic signals with frequencies up to 100 Hz.

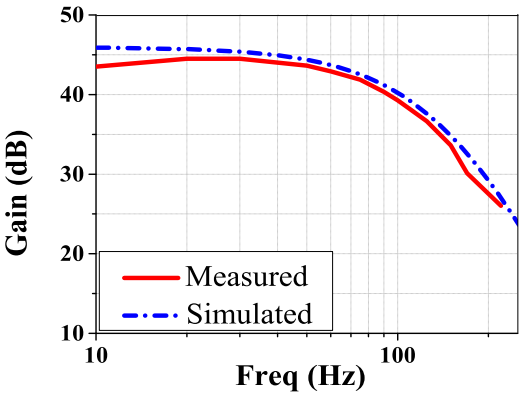

FIGURE 6. Measured and simulated gain vs. frequency of the analog circuit shown in Fig. 5.

In order to verify the reliability of using our sensing system in detecting vibrations and making useful interpretations based on the generated data, we conducted a simple test using our geophone sensing node. The node was placed on one end of a long table and on the other end of the table a small vibration source was placed. The employed vibration source was a commercial neck massager [25] that rotates at a fixed frequency of around 1 Hz with fixed intensity. The generated peak voltage from the GSN due to the surface acoustic wave generated by the massager was recorded for a range of

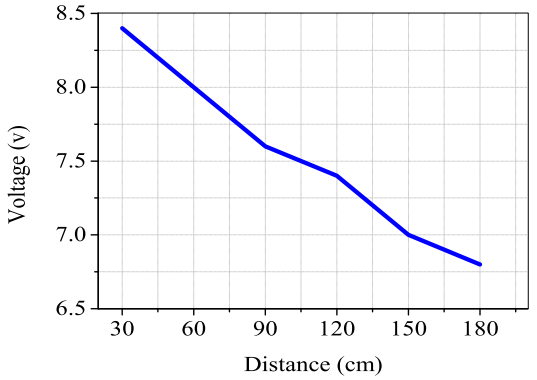

FIGURE 7. A plot of the peak generated geophone node voltage due to the surface acoustic wave generated by the vibration source (massager) vs. the distance between the geophone node and the vibration source, showing an inverse relationship between the peak voltage and distance.

distances between the GSN and the vibration source, and a plot of peak detected voltage vs. distance is shown in Fig. 7. As the figure shows, the magnitude of the peak voltage is inversely related to the distance between the geophone and the vibration source, demonstrating the reliability of using the geophone signal in interpreting the distance between the geophone and the vibration source.

C. THE MICROCOMPUTER AND ADC - SAMPLING AND DIGITIZATION

After the raw analog signal is filtered and amplified, it needs to be sampled at a rate of 500 samples/second and quantized at a resolution of 24 bits/sample in order to prepare it for digital transmission and to enable its storage to the on-board memory in digital format. In cabled systems, this step would be done near the recording station, however, in wireless systems, it is critical for this step to take place within the sensor node itself, so that the data can be sent in digital format over the wireless link to ensure minimal errors during transmission. In order to achieve this, an on-board microcomputer is employed along with a high precision ADC. The microcomputer is powered using a solar power bank, as shown in Fig. 4 earlier.

The used microcomputer is a Raspberry Pi single-board computer, which is a small size low-cost computer. A Raspberry Pi 2 - Model B is used as it offers favorable power efficiency in comparison with the other models that also offer compatibility with high precision Analog-to-Digital/Digital-to-Analog boards. As discussed earlier, a 24-bit ADC will be employed as it is capable of distinguishing 16,777,216 (2^{24}) different voltage levels within a narrow voltage range from 0 to 5 volts, which means that each level represents approximately 0.3 μV; satisfying the high-resolution requirements of seismic surveys. It is important to note that each time a sample is sampled and digitized, the microcomputer adds a timestamp to it to preserve the time at which it was sampled, which happens to be critical information that would be needed in processing the data later on, in order to enable its appropriate interpretation. After labelling the received data from the ADC with a time stamp, the microcomputer is employed to perform two essential functions in parallel; saving the data to an on-board memory (a micro SD card) as a CSV file and sending the data to the communication module of the sensor node in order to be transmitted wirelessly to the gateway in real-time. All these functions are programmed using C language because of its high performance. The flow chart in Fig. 8 shows the flow of the code used in the Raspberry Pi.

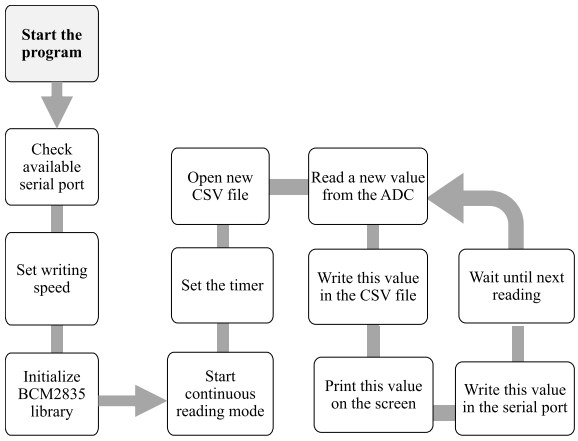

FIGURE 8. The flow of functions that are executed by the C-language code implemented in the Raspberry Pi Microcomputer.

IV. WIRELESS COMMUNICATION MODULE

This section is aimed at discussing how the digital data collected by the data acquisition module is transmitted wirelessly to the gateway. This section is divided into three sub-sections. The transmitter configuration sub-section discusses how the collected seismic data is transmitted wirelessly from the geophone node to gateway using the XBee (S2C-802.15.4) RF module [19]. The receiver configuration sub-section details how information from the node is received at gateway. The last sub-section presents the reconfigurable antenna design, structure, and experimental performance characterization.

A. TRANSMITTER CONFIGURATION

To wirelessly transmit high resolution data from the GSN to the gateway, a technology that can support a reasonable data rate with low power consumption and wide coverage is required. The XBee RF module (S2C-802.15.4) [19] which possess a data rate of up to 250 *kbit/s* and consumes only 25% of the power consumed by standard Wi-Fi; is employed. The operating frequency of this module is 2.4 *GHz*, which is compatible with several wireless systems. Consequently, A reconfigurable directional antenna is designed to operate at this frequency with matching bandwidth that supports this transmission rate, the detailed design of which is postponed to Sub-Section C.

There are two different modes for operating the XBee module: Application Transparent (AT) mode and Application Programming Interface (API) mode [26]. The AT mode is

termed "transparent" because within it; information is passed along exactly as it is received.

In API mode, a protocol determines the way information is exchanged. Data communicated in packets is commonly called API frames. This mode allows users to create extensive networks and is more appropriate for sensor networks to perform tasks such as collecting data from multiple locations and controlling devices remotely. An Arduino micro-controller is used to control the antenna reconfigurability and the XBee module operation in API mode. A multi-point to multi-point scenario, where several nodes send data to different coordinators (i.e., getaways) is required. An addressing mechanism is utilized to separate the data received from different nodes. Fig. 9 illustrates the network setup used for this topology with 4 XBee modules and 4 Arduinos. The nodes select a coordinator and transmit data, and the coordinator separates data coming from each node and stores it.

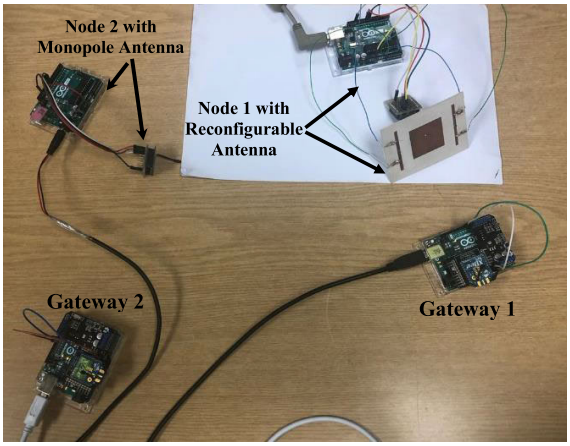

FIGURE 9. Network setup used to test the proof-of-concept smart wireless geophone sensor network in a multi-point to multi-point wireless communication scenario.

The frame structure is compiled in Table 1, where bytes inside the frame are represented in hexadecimal coding [27]. The first byte is the start delimiter, which indicates the start position of the frame. Its value is always assigned "7E" to be recognized as start of frame. The second and third bytes provide the length of the frame excluding the start delimiter. The fourth byte represents the frame type, which in this case is the API mode, and the standard value of which is "92". The actual data sent starts with byte number 5. The final byte represents the checksum, which enables the receiver to detect whether the sent packet is fully received or not. After preparing the information in frames, quadrature phase shift keying (QPSK) modulation is initiated automatically by the RF module.

TABLE 1. Data representation in the frame structure that is sent from the GSN to the gateway unit.

Start delimiter	Length		Frame data								Checksum
			Frame type	Data							
1	2	3	4	5	6	7	8	9	10	..... n	n+1
7E	MSB	LSB	API	Specific data							

B. RECEIVER CONFIGURATION

Each time the receiver gateway gets a packet from the nodes, the XBee passes the frame serially to the Arduino micro-controller. The program checks the validity of the packet using checksum; if it is valid, the program extracts both the 64-bit source address and the data from the frame. Moreover, based on the source address, it separates data received from each node and saves it in a string, then communicates it serially to the computer via USB cable. Concurrently, a software program is used to save all data arriving from the same USB port to an excel sheet where each node is assigned to a specific column. The time stamp is also recorded to generate a real-time plot for the data being received from each sensor node.

C. ANTENNA DESIGN AND RECONFIGURABILITY

Commercially available geophone systems [11]–[12] employ conventional monopole antennas that suffer from low gain, and this affects their ability to transmit data over long distances. Due to this low gain, a large number of gateways is required. This work proposes, for the first time in literature, the use of directional antennas in the GSNs, with high gain and reconfigurable radiations patterns, in order to enhance the communication range between the GSNs and the gateways. This would result in increasing an individual gateway's coverage area and hence allows a reduction in the total number of gateways needed to cover a whole survey area. Numerous research reports have demonstrated the leverage of reconfigurable antennas over omni-directional antennas [28]–[30], however, in this work we will demonstrate their leverage for application in wireless geophone sensor networks.

The employed antenna needs to be able to support the carrier frequency and to provide enough bandwidth for the required data rate. With these design requirements in mind, a pattern reconfigurable antenna was designed and fabricated and is shown in Fig. 10, showing its top and bottom views along with its prototype. For our reconfigurable antenna, the measured matching bandwidth was around 200 *MHz*, which is much higher than the needed bandwidth, allowing flexibility for future increase in the data rate.

The reconfigurable antenna was printed on a 90 mm by 85 mm dielectric material (Rogers RO3003) with a dielectric constant of 3 and thickness of 1.52 mm. The top layer consists of the radiating elements (square patch and two parasitic elements placed side by side) and four biasing lines to control PIN diodes, which act as electronic switches. Each PIN diode is controlled by two biasing lines, one serves as a DC supply and the other as ground. The bottom layer consists of a printed line which serves as a partial ground plane. The antenna has the following dimensions $L_r = 49$ mm, $L_m = 44$ mm, $L_S = 90$ mm, $W_p = 85$ mm, $S = 30.76$ mm, $g = 14$ mm, $w = 3$ mm, $d = 3$ mm, $W_S = 34.7$ mm.

The antenna uses two PIN diodes that are controlled by a microcontroller; this may result in four different modes of radiation. Since the first two modes (both OFF and both ON)

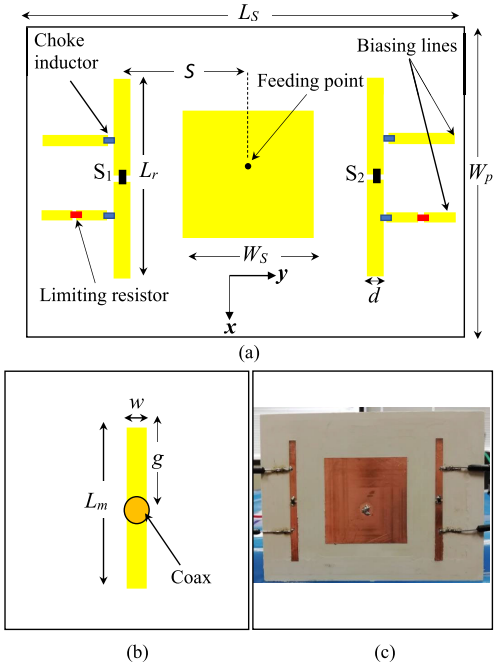

FIGURE 10. Structure of the pattern reconfigurable antenna. (a) Top view, (b) bottom view, and (c) fabricated prototype.

TABLE 2. Switching modes of the reconfigurable antenna.

Modes	Scan angle	S_1	S_2
1	90°	1	0
2	-90°	0	1
3	0°	0	0

have similar radiation patterns, they are considered as one mode with both diodes OFF to save power. Table 2 shows the switching states of the PIN diodes.

An Arduino microcontroller is programmed to select the direction that has a higher received signal strength indicator (RSSI) level and switch the reconfigurable antenna to that direction. The mechanism of decision making is that a broadcast message is conveyed to all nodes from the gateway to search for a suitable path for sending the data. Consequently, the antenna beam of each individual sensor node scans all directions by controlling the state of its PIN diodes. The microcontroller stores the RSSI values for each gateway for all modes and compares them to select the gateway associated with the largest RSSI value. Finally, the address of the chosen gateway is set and the node gets ready for transmission.

One of the parameters that control the switching ability of the antenna is the width of the ground plane [31]. Two PIN diodes HPND-4005 (S_1-S_2) are used as switches as shown in Fig. 10. The ON-state of this diode is modelled as a series-RLC with R = 4.7 Ω, L = 0.15 *nH*, and C = 0, while the OFF-state is modelled as a parallel-RLC with R = 7 *M*Ω, L = 0 *H*, and C = 0.017 *pf*. A 68 *nH* inductor and 500 Ω resistor were placed on the biasing lines to serve as RF choke and a current limiting resistor, respectively. Figs. 11(a-c) depict the radiation patterns of all switching modes in the H-plane. It is evident that the antenna can scan the beam in

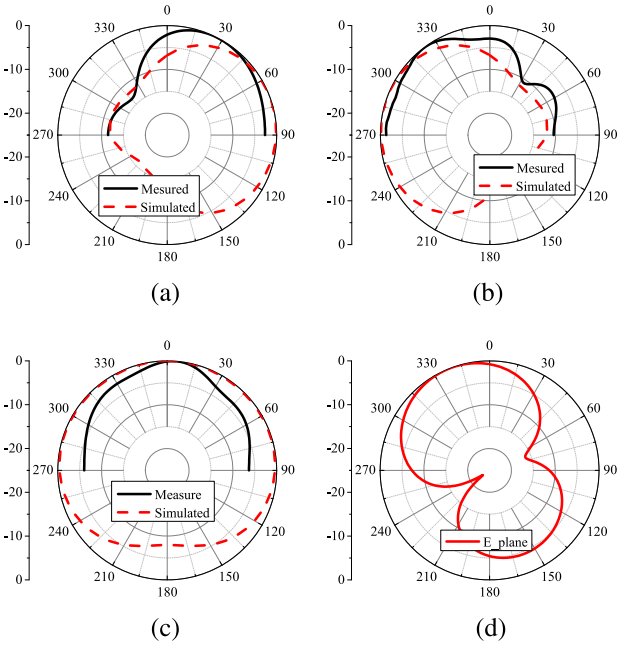

FIGURE 11. The simulated and measured 2D H-plane (*yz*-plane) radiation patterns of the pattern reconfigurable antenna: (a) Mode 1 with the main beam at 90° (b) Mode 2 with the main beam at −90° (c) Mode 3 with the main beam at 0° (d) E-plane for all modes.

three different directions (i.e. −90°, 0° and 90°). Moreover, Fig. 11(d) shows the simulated E-plane radiation pattern, which is found to be the same for all switching modes. Good agreement between the measured and simulated results are observed. Fig. 12 depicts the simulated and measured reflection coefficients of the antenna. These figures reveal that the antenna has acceptable matching (below −10 dB) for all switching modes. The antenna directivity and impedance bandwidth range from 6 - 7 dB and 4% - 6%, respectively, for all switching modes. This achieved directivity is more than twice that of a conventional omnidirectional monopole antenna, which is about 1.7 dB.

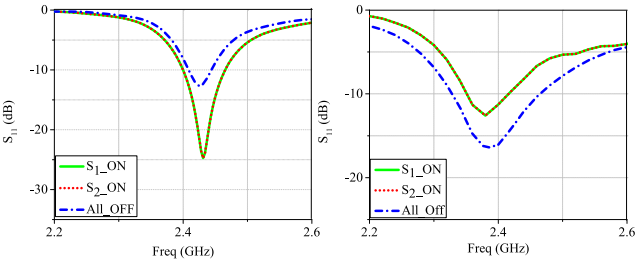

FIGURE 12. (a) Simulated and (b) measured reflection coefficients of the pattern reconfigurable antenna for all switching modes.

V. SYSTEM INTEGRATION, PACKAGING AND TESTING

Packaging is an essential aspect in sensing systems design in order to integrate the different system components and ensure that the performance of the system is not affected by environmental factors. The 3-D online drawing tool (Tinkercad) [32] was utilized to design a 3-D model of the system package.

To ensure portability of the whole system, the minimum possible size of each individual component was measured and the final dimensions of the outer package were chosen to be $18 \times 16 \times 13\ cm^3$. The package was fabricated by 3D printing and the system components were placed within the package as per the design. Fig. 13 shows the distribution of devices inside the box. It is important to note that since the current system is only a first proof-of-concept prototype, the package shape and ergonomics are not fully optimized and there is plenty of room for further enhancement in future generations of the system.

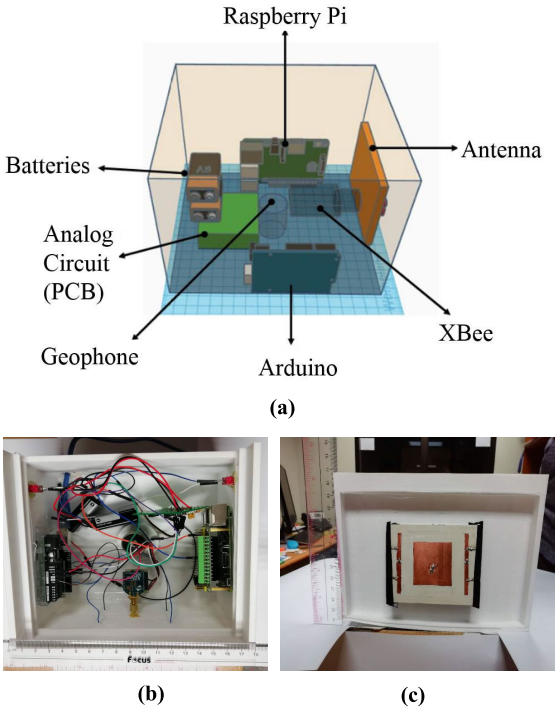

FIGURE 13. Package of the GSN. (a) 3D model as produced in Tinkercad CAD modelling software. (b) Top view of the GSN (real prototype). (c) Side view showing the antenna (real prototype). Note that the solar power bank is not visible as it is positioned on the top lid, which has been removed here to allow visualization of the components inside the package.

A. OUTPUT RESULT OF THE OVERALL SYSTEM

The wireless seismic data acquisition system was successfully implemented and tested. Fig. 14 shows the final system in a lab bench test setup, where the GSN was placed within a box of sand, while the gateway was connected to a laptop for real-time plotting of the received results. The geophone was excited by continuously tapping (by hand) the table - on top of which the system was placed - with different forces, and the data was received wirelessly at the gateway. Fig. 15 shows the system output obtained when tapping the table; it is evident that different forces give different amplitudes.

In the multimedia supplementary materials appended to this article, Video 2 shows another experimental lab bench test setup, where the individual components are removed outside of the package and the output waveform acquired at

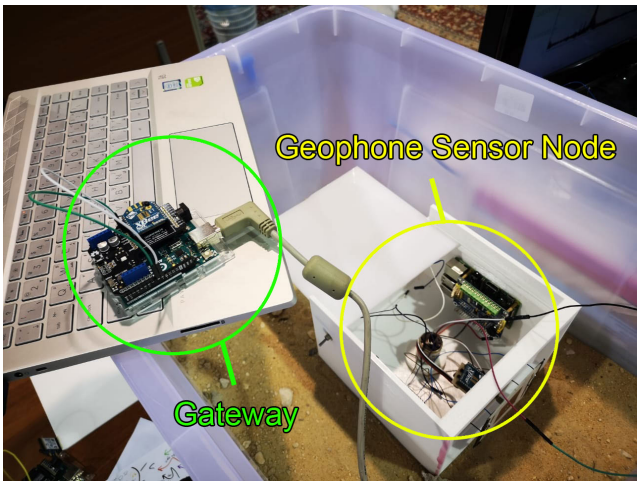

FIGURE 14. Lab bench test setup of the complete proof-of-concept sensor network, composed of the smart GSN placed in a sand box, and a gateway connected to a laptop. The analog Circuit (PCB) and all batteries were temporarily removed from the package to allow visualization of the geophone sensor positioning within the package.

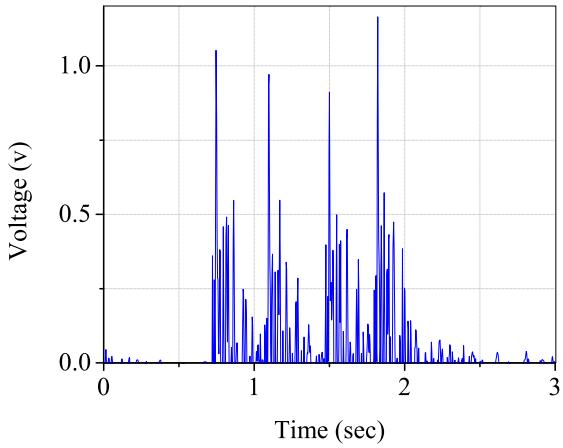

FIGURE 15. Full system output voltage received wirelessly at the gateway when tapping the table - on top of which the system was placed - with different forces (see Video 2 in the multimedia supplementary materials appended to this article).

the GSN is plotted in real-time concurrently with the received data at the gateway side. The video shows clearly how the signal is acquired, digitized and sent wirelessly in real-time to the gateway, demonstrating the real-time agreement between the collected signal at the geophone node and the received signal at the gateway.

B. IMPACT OF THE RECONFIGURABLE ANTENNA ON THE COMMUNICATION RANGE

The main novelty of the proposed smart GSN was its capability to locate the nearest gateway and direct its radiation beam towards the direction of that specific gateway, by means of a reconfigurable directional antenna, in order to efficiently utilize the power used in sending the data over the communication link. To verify the leverage of our proposed reconfigurable RF-front end, the implemented smart GSN with this reconfigurable directional antenna was tested (both indoors and outdoors) and was compared with a similar GSN that

employs a conventional monopole antenna instead, similar to antennas currently employed in the commercial wireless seismic data acquisition systems [11], [12].

The components used in this test experiment were the same components used for the multi-point to multi-point communication test scenario, which were previously shown in Fig. 9. The indoor test was conducted in the KFUPM Electrical Engineering building, while the outdoor test was conducted in the KFUPM football stadium. The test was conducted by sending a message to the GSN from the gateway and then measuring the strength of the received signal (i.e., RSSI) at the GSN over a range of different distances between the GSN and the gateway. The results from this test are presented in Fig. 16. It is evident that for the indoor environment (Fig. 16(a)), the two GSNs have almost equal performance. This is due to multi-reflections from the walls and other objects within the path between the GSN and the gateway, which would deteriorate any directional advantage offered by the reconfigurable antenna, as expected.

On the other hand, for the outdoor environment which is more relevant for seismic surveys, as seen in Fig. 16(b), the GSN with the reconfigurable directional antenna clearly outperforms the GSN with a conventional monopole antenna. The strength of the received signal at the smart GSN is consistently 10-20 dBm greater than the signal received at the GSN with a conventional monopole antenna.

As can be seen from Fig. 16(b), and assuming a minimum required signal strength for data reception of −100 dBm, the GSN with the reconfigurable antenna was able to reach to a distance of 200 m, while the GSN with a conventional monopole antenna was only able to reach a distance of 160 m. This represents a 25% enhancement in the maximum communication range between the GSN and the gateway.

However, In order to further appreciate the impact of this extended range enhancement on the network level, it is important to revisit how a seismic survey, based on a wireless geophone sensor network, is conducted. Usually, active seismic surveys are conducted over areas of potential hydrocarbon traps that can span regions as wide as tens of kilometers by tens of kilometers, and which require a very large number of remotely distributed GSNs in order to cover such a large area. In order for these geophone sensors to be able to relay their collected data back to the central data collection center, they need to first send their data to local gateways that usually cover a limited area within the total area under survey. The number of gateways needed to cover the full survey area would scale based on the maximum coverage area of each individual gateway. Gateways are usually more advanced wireless modules than individual sensor nodes as they need to communicate with a large number of sensor nodes concurrently, and also need to send the aggregate data from all of these nodes to a central recording station or to a nearer gateway to the central recording station, depending on the employed network architecture. Hence, it is highly favorable that the number of gateways needed to cover a specific survey area be reduced. In order to achieve this, an important means

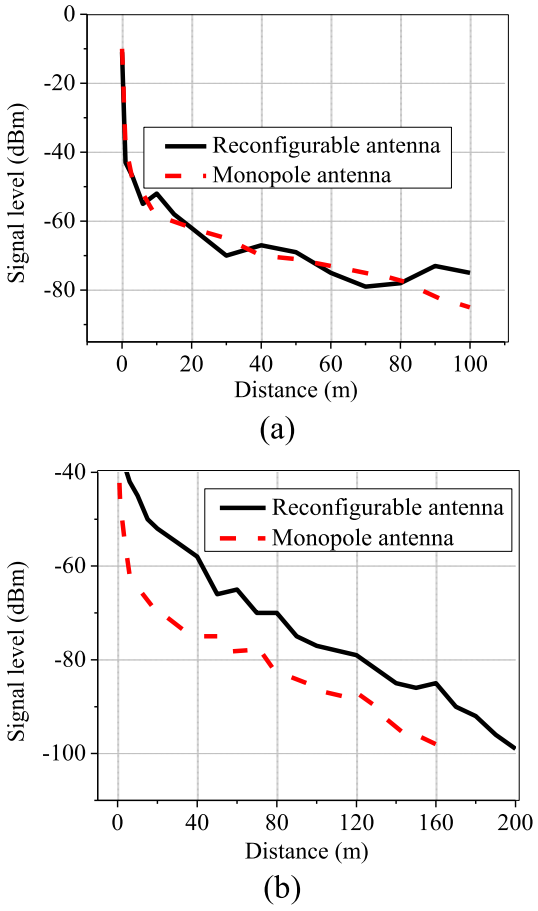

FIGURE 16. RSSI comparison between the signal strength received from the gateway at the GSN with the reconfigurable antenna and the GSN with a conventional monopole antenna in (a) indoor, and (b) outdoor environments.

would be to maximize the coverage area of an individual gateway. This latter endeavour can be achieved by increasing the distance over which a gateway can communicate with a sensor node, and we will refer to this distance here by (r). As was demonstrated earlier, using our smart sensor node r was increased by a factor of 25 % by means of the directional reconfigurable antenna. This increase in the communication range (r) results in enhancing the maximum coverage area of the gateway (A) by a factor of more than 56% ($A = \pi r^2$). This enhancement in the coverage area is illustrated in Fig. 17.

C. NETWORK-LEVEL CONSIDERATIONS

After demonstrating the impact of using reconfigurable antennas in the GSNs on extending the transmission range to the gateway, it is essential, prior to network-level implementation, to conduct a comprehensive network-level analysis and simulation. A system-level simulation in [33] of the performance of wireless geophone sensor networks was conducted, considering multiple access schemes among multiple wireless GSNs. Additionally, the authors in [33] have further considered the impact of co-channel interference (CCI) through numerical simulations. This can be further corroborated with experimental implementation focusing on

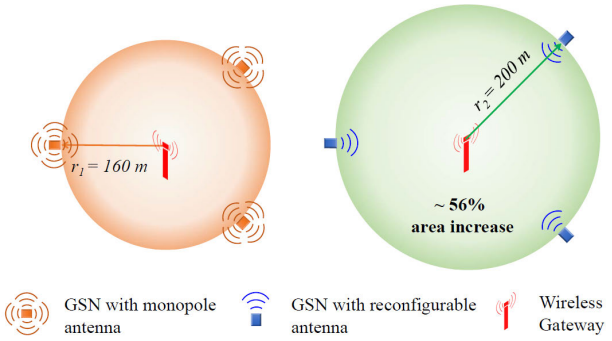

FIGURE 17. Schematic representation illustrating the increase in area coverage of a gateway, according to the maximum communication distance with a GSN, comparing the case when communicating with GSNs that have monopole antennas (left) vs. GSNs with reconfigurable antennas (right).

real-time seismic acquisition in dense networks and taking into consideration CCI and relevant impairments. Generally, directional antennas can provide coverage enhancements; however, in some set-ups, this may come at the cost of non-negligible CCI levels, which highly depend on the specific layout of gateways/sink nodes. For example, in large-scale random wireless networks with random access schemes, directional antennas can experience CCI from out-of-cell base stations or nodes [34], [35]. One way to mitigate the induced interference in such random set-ups or layouts is adopting smart algorithms which identify the level of interference, and/or using proper interference-free scheduling capabilities. For example, in IEEE 802.22 and IEEE 802.16h [36], such schemes can reduce and relatively mitigate CCI. Further reconfiguration/rearrangement of the antenna radiation pattern might be further explored to limit such impairments. On the other hand, in fixed multi-point communication systems - similar to geophone sensor networks employed in active seismic surveys, antenna directivity is a common approach to control CCI, with the goal of maximizing the frequency reuse and limiting the interference by controlling the radiated emissions with careful frequency spectrum planning. An interesting research problem can be to explore the minimization of CCI exploiting the capability of controlling/steering the radiation of antennas in wireless geophone networks, given the large-scale nature of the network and that wireless GSNs are stationary/fixed.

VI. CONCLUSION

This paper presents the design and implementation of a fully functional smart wireless geophone sensor network for seismic data acquisition. The impact of employing the proposed system in active seismic surveys, based on wireless geophone sensor networks, was demonstrated through the implementation of a proof-of-concept network that comprises a smart wireless sensor node and a gateway unit. The smart feature of the geophone sensor node was achieved by means of a pattern reconfigurable antenna whose radiation can be switched in three different directions ($-90°$, $0°$ and $90°$), in order to direct its radiation power in the direction of the nearest gateway. The implemented system successfully captured seismic data from the geophone sensor and transmitted it wirelessly to the gateway unit in real-time; while being powered with a solar power bank. It was evident that the smart sensor node with the reconfigurable antenna achieves enhanced performance when compared with a sensor node with a conventional monopole antenna, by achieving a 25% enhancement in the communication range with the gateway. This enhancement reflects in enlarging the coverage area of a single gateway - communicating with such a smart class of geophone sensor nodes - by more than 56%. Our presented smart wireless geophone sensor network design, employing the reconfigurable directional antennas, promises to bring wireless geophone sensor networks a step closer towards commercial maturity, which can have a great impact on a wide range of major industries, such as the global oil and gas industry.

ACKNOWLEDGMENT

The authors would like to thank M. S. Sharawi and A. H. Muqaibel for their valuable comments and feedback on the manuscript. This work was supported by the Center for Energy and Geo-Processing (CeGP) at King Fahd University of Petroleum and Minerals (KFUPM), Dhahran, Saudi Arabia, under grant number GTEC1802.

REFERENCES

[1] S. Savazzi and U. Spagnolini, "Wireless geophone networks for high-density land acquisition: Technologies and future potential," *Geophysics*, vol. 27, pp. 882–886, Jul. 2008.
[2] S. Savazzi, U. Spagnolini, L. Goratti, D. Molteni, M. Latva-aho, and M. Nicoli, "Ultra-wide band sensor networks in oil and gas explorations," *IEEE Commun. Mag.*, vol. 51, no. 4, pp. 150–160, Apr. 2013.
[3] D. Crice, P. Flood, and E. Walthinsen, "Cableless seismic systems for near surface geophysics," in *Proc. Symp. Appl. Geophys. Eng. Environ. Problems*, Mar. 2015, pp. 465–468.
[4] M. Picozzi, C. Milkereit, S. Parolai, K.-H. Jaeckel, I. Veit, J. Fischer, and J. Zschau, "GFZ wireless seismic array (GFZ-WISE), a wireless mesh network of seismic sensors: New perspectives for seismic noise array investigations and site monitoring," *Sensors*, vol. 10, no. 4, pp. 3280–3304, 2010.
[5] G. Koc and K. Yegin, "Hardware design of seismic sensors in wireless sensor network," *Int. J. Distrib. Sensor Netw.*, vol. 9, no. 9, Sep. 2013, Art. no. 640692.
[6] M. J. Rubin, M. B. Wakin, and T. Camp, "Lossy compression for wireless seismic data acquisition," *IEEE J. Sel. Topics Appl. Earth Observ. Remote Sens.*, vol. 9, no. 1, pp. 236–252, Jan. 2016.
[7] S. K. V. Sudarshan, V. Montano, A. Nguyen, M. McClimans, L. Chang, R. R. Stewart, and A. T. Becker, "A heterogeneous robotics team for large-scale seismic sensing," *IEEE Robot. Autom. Lett.*, vol. 2, no. 3, pp. 1328–1335, Jul. 2017.
[8] V. A. Reddy, G. L. Stueber, and S. I. Al-Dharrab, "Energy efficient network architecture for seismic data acquisition via wireless geophones," in *Proc. IEEE Int. Conf. Commun. (ICC)*, May 2018, pp. 1–5.
[9] V. A. Reddy, G. L. Stuber, and S. I. Al-Dharrab, "High-speed seismic data acquisition over mm-wave channels," in *Proc. IEEE 88th Veh. Technol. Conf. (VTC-Fall)*, Aug. 2018, pp. 1–5.
[10] A. Othman, W. Mesbah, N. Iqbal, S. Al-Dharrab, A. Muqaibel, and G. Stuber, "Sum-rate maximization for wireless seismic data acquisition systems," in *Proc. SEG Tech. Program Expanded Abstr.*, Aug. 2018, pp. 181–185.
[11] *Land Seismic Acquisition System*. Accessed: Feb. 17, 2020. [Online]. Available: https://wirelessseismic.com/
[12] *Land Seismic Acquisition System*. Accessed: Feb. 17, 2020. [Online]. Available: http://www.sercel.com/Pages/default.aspx/

[13] G. J. Vermeer, *3D Seismic Survey Design*, 2nd ed. London, U.K.: Society of Exploration Geophysicists, 2012.
[14] S. Mitra, "Fault-propagation folds: Geometry, kinematic evolution, and hydrocarbon traps (1)," *AAPG Bull.*, vol. 74, no. 6, pp. 921–945, Jun. 1990.
[15] W. Song, F. Li, M. Valero, and L. Zhao, "Toward creating a subsurface camera," *Sensors*, vol. 19, no. 2, p. 301, Jan. 2019, doi: 10.3390/s19020301.
[16] W.-Z. Song, R. Huang, M. Xu, B. Shirazi, and R. LaHusen, "Design and deployment of sensor network for real-time high-fidelity volcano monitoring," *IEEE Trans. Parallel Distrib. Syst.*, vol. 21, no. 11, pp. 1658–1674, Nov. 2010.
[17] F. Li, M. Valero, Y. Cheng, T. Bai, and W. Song, "Distributed sensor networks based shallow subsurface imaging and infrastructure monitoring," *IEEE Trans. Signal Inf. Process. Netw.*, vol. 6, pp. 241–250, 2020.
[18] J. Clemente, F. Li, M. Valero, A. Chen, and W. Song, "ASIS: Autonomous seismic imaging system with *in situ* data analytics and renewable energy," *IEEE Syst. J.*, vol. 14, no. 1, pp. 1277–1284, Mar. 2020.
[19] *Digi XBEE S2C-802.15.4 RF Modules*. Accessed: Feb. 17, 2020. [Online]. Available: https://www.digi.com/pdf/ds_xbee-s2c-802-15-4.pdf
[20] S. Zhang, G. H. Huff, J. Feng, and J. T. Bernhard, "A pattern reconfigurable microstrip parasitic array," *IEEE Trans. Antennas Propag.*, vol. 52, no. 10, pp. 2773–2776, Oct. 2004.
[21] W. Lin, H. Wong, and R. W. Ziolkowski, "Circularly polarized antenna with reconfigurable broadside and conical beams facilitated by a mode switchable feed network," *IEEE Trans. Antennas Propag.*, vol. 66, no. 2, pp. 996–1001, Feb. 2018.
[22] S. Gaya, O. Sokunbi, S. I. Sheikh, and H. Attia, "Monopole antenna with beam scanning in both end-fire and broadside directions," in *Proc. IEEE Radio Wireless Symp. (RWS)*, Antonio, TX, USA, Jan. 2020.
[23] S.-L. Chen, P.-Y. Qin, W. Lin, and Y. J. Guo, "Pattern-reconfigurable antenna with five switchable beams in elevation plane," *IEEE Antennas Wireless Propag. Lett.*, vol. 17, no. 3, pp. 454–457, Mar. 2018.
[24] *Geophone—SM-24*. Accessed: Feb. 17, 2020. [Online]. Available: https://www.sparkfun.com/products/11744
[25] *Deep Tissue Neck, and Back Massager*. Accessed: Feb. 17, 2020. [Online]. Available: https://www.amazon.com/FIVE-FS8801-Kneading-Shoulder-Massager/dp/B00O2I40SE/ref=sr_1_50?keywords=Neck+and+Back+Massager&qid=1572335975&sr=8-5
[26] *Xbee Operating Modes*. Accessed: Feb. 17, 2020. [Online]. Available: https://www.digi.com/resources/documentation/Digidocs/90001942-13/concepts/c_xbee_comparing_at_api_modes.htm?TocPath=How%20XBee%20devices%20work%7CSe%rial%20communication%7C_____2
[27] D. Chen, G. Li, J. Wang, J. Chen, W. He, Y. Fan, T. Deng, and P. Wang, "A micro electrochemical seismic sensor based on MEMS technologies," *Sens. Actuators A, Phys.*, vol. 202, pp. 85–89, Nov. 2013.
[28] X. Ding and B.-Z. Wang, "A novel wideband antenna with reconfigurable broadside and endfire patterns," *IEEE Antennas Wireless Propag. Lett.*, vol. 12, pp. 995–998, 2013.
[29] S. Gaya, H. Attia, S. I. Sheikh, A. Mahmoud, and M. S. Sharawi, "A Yagi-Uda pattern reconfigurable antenna for WiMAX application," in *Proc. IEEE Int. Symp. Antennas Propag. USNC-URSI Radio Sci. Meeting*, Jul. 2019, pp. 679–680.
[30] M. S. Khan, A.-D. Capobianco, S. M. Asif, A. Iftikhar, B. D. Braaten, and R. M. Shubair, "A pattern reconfigurable printed patch antenna," in *Proc. IEEE Int. Symp. Antennas Propag. (APSURSI)*, Jun. 2016, pp. 2149–2150.
[31] S. Gaya, R. Hussain, M. S. Sharawi, and H. Attia, "Pattern reconfigurable Yagi-Uda antenna with seven switchable beams for WiMAX application," *Microw. Opt. Technol. Lett.*, vol. 62, no. 3, pp. 1329–1334, 2020.
[32] *3D Online CAD Design*. Accessed: Feb. 17, 2020. [Online]. Available: https://www.tinkercad.com
[33] V. A. Reddy, G. L. Stuber, S. Al-Dharrab, W. Mesbah, and A. H. Muqaibel, "A wireless geophone network architecture using IEEE 802.11af with power saving schemes," *IEEE Trans. Wireless Commun.*, vol. 18, no. 12, pp. 5967–5982, Dec. 2019.
[34] C. Psomas, M. Mohammadi, I. Krikidis, and H. A. Suraweera, "Impact of directionality on interference mitigation in full-duplex cellular networks," *IEEE Trans. Wireless Commun.*, vol. 16, no. 1, pp. 487–502, Jan. 2017.
[35] A. M. Hunter, J. G. Andrews, and S. Weber, "Transmission capacity of ad hoc networks with spatial diversity," *IEEE Trans. Wireless Commun.*, vol. 7, no. 12, pp. 5058–5071, Dec. 2008.
[36] J. Sydor, "A proposal to standardize directive antennas and highly sectored cellular hub systems for outdoor point to multipoint applications: IEEE 802.16.3 phy layer," IEEE 802.16.3 Broadband Wireless Access Work. Group, Tech. Rep., 2000. [Online]. Available: https://ieeexplore.ieee.org/document/7562988

HUSSEIN ATTIA (Member, IEEE) received the Ph.D. degree in electrical and computer engineering from the University of Waterloo, Waterloo, ON, Canada, in 2011.

He worked as a Research Engineer with the Coding and Signal Transmission Laboratory, University of Waterloo, from March 2011 till July 2013. He was granted a Postdoctoral Fellowship at Concordia University, Montreal, QC, Canada, from August 2014 to July 2015. Also, he was a Visiting Scholar with University de Quebec (INRS), from August 2015 to December 2015 and from June 2017 to August 2017. He is currently an Assistant Professor with the King Fahd University of Petroleum and Minerals (KFUPM). He published 80 journal and conference papers. His research interests include millimeter-wave high-gain and wide-band antennas, analytical techniques for electromagnetic modeling, and engineered magnetic metamaterials. During his Ph.D. program, he received the University of Waterloo Graduate Scholarship for excellence in research and coursework, in 2009. He was a finalist in the Student Paper Competition of the 2011 IEEE AP-S International Symposium on Antennas and Propagation. He ranked first among all B.Sc. students of electronics and communication engineering, Zagazig University, Egypt, in 1999.

SAGIRU GAYA received the B.Sc. degree (Hons.) in electrical engineering from the Kano University of Science and Technology, Nigeria, in 2016. He is currently pursuing the M.Sc. degree in electrical engineering with the King Fahd University of Petroleum and Minerals (KFUPM), Dhahran, Saudi Arabia.

He published multiple journal and conference papers in the area of reconfigurable antennas for different wireless applications. He is an Active Member of the Applied Electromagnetics Lab, KFUPM.

ABDULLAH ALAMOUDI received the bachelor's degree in electrical engineering from the King Fahd University of Petroleum and Minerals (KFUPM), Dhahran, Saudi Arabia, in 2019. He was a Senior Undergraduate Student in electrical engineering with KFUPM, at the time of conducting this work. He was the student coordinator of the Electronics Team working on the data acquisition module.

FAHAD M. ALSHEHRI received the bachelor's degree in electrical engineering from King Fahd University of Petroleum and Minerals (KFUPM), Dhahran, Saudi Arabia, in 2019. He was a Senior Undergraduate Student in electrical engineering with KFUPM, at the time of conducting this work. He was the Student Coordinator of the Communications Team working on the communications module.

ABDULRAHMAN AL-SUHAIMI received the bachelor's degree in electrical engineering from the King Fahd University of Petroleum and Minerals (KFUPM), Dhahran, Saudi Arabia, in 2019. He was a Senior Undergraduate Student in electrical engineering with KFUPM, at the time of conducting this work. He was part of the Electronics Team working on the data acquisition module.

NAWAF ALSULAIM received the bachelor's degree in electrical engineering from the King Fahd University of Petroleum and Minerals (KFUPM), Dhahran, Saudi Arabia, in 2019. He was a Senior Undergraduate Student in electrical engineering with KFUPM, at the time of conducting this work. He was part of the Electronics Team working on the data acquisition module.

AHMAD M. AL NASER received the bachelor's degree in electrical engineering from the King Fahd University of Petroleum and Minerals (KFUPM), Dhahran, Saudi Arabia, in 2019. He was a Senior Undergraduate Student in electrical engineering with KFUPM, at the time of conducting this work. He was part of the Communications Team working on the communications module.

MOHAMAD AGHYAD JAMAL EDDIN received the bachelor's degree in electrical engineering from the King Fahd University of Petroleum and Minerals (KFUPM), Dhahran, Saudi Arabia, in 2020. He was a Senior Undergraduate Student in electrical engineering with KFUPM, at the time of conducting this work. He was part of the Communications Team working on the communications module.

ABDULLAH M. ALQAHTANI received the bachelor's degree in electrical engineering from the King Fahd University of Petroleum and Minerals (KFUPM), Dhahran, Saudi Arabia, in 2019. He was a Senior Undergraduate Student in electrical engineering with KFUPM, at the time of conducting this work. He was part of the Communications Team working on the communications module.

JHONATHAN PRIETO ROJAS (Member, IEEE) received the bachelor's degree in electronics engineering from the National University of Colombia, in 2009, the master's and Ph.D. degrees in electrical engineering from the King Abdullah University of Science and Technology (KAUST), in 2010 and 2014, respectively. He joined KFUPM as an Assistant Professor with the Electrical Engineering Department, in Fall 2015. He has published more than 25 journal articles in renowned journals and more than 30 conference papers.

SUHAIL AL-DHARRAB (Senior Member, IEEE) received the B.Sc. degree in electrical engineering from the King Fahd University of Petroleum and Minerals, Dhahran, Saudi Arabia, in 2005, and the M.A.Sc. and Ph.D. degrees in electrical and computer engineering from the University of Waterloo, Waterloo, ON, Canada, in 2009 and 2013, respectively. From 2005 to 2007, he was a Graduate Assistant with the Electrical Engineering Department, King Fahd University of Petroleum and Minerals. In 2015, he was a Visiting Professor with the School of Electrical and Computer Engineering, Georgia Institute of Technology, Atlanta, USA. He is currently an Assistant Professor with the Electrical Engineering Department and the Assistant Dean of Research with the King Fahd University of Petroleum and Minerals. His research interests span topics in the areas of wireless communication systems, underwater acoustic communication, digital signal processing, and information theory.

FERAS AL-DIRINI (Member, IEEE) recieved the B.Sc. degree (Hons.) in electronics engineering from Princess Sumaya University for Technology, Jordan, in 2011, and the Ph.D. degree in electrical and electronic engineering from The University of Melbourne, Australia, in 2015.

He joined the Electrical Engineering Department, KFUPM, in September 2017, as an Assistant Professor, coming from the University of Melbourne in Australia, where he has been working with the Electrical and Electronic Engineering Department, since 2015. From 2009 to 2010, he was an Exchange Student with the University of Illinois at Urbana–Champaign, USA, and in the Summer of 2009, he was a Research Intern with the Institute for Microsystems Technology, Technical University of Hamburg, Harburg, Germany. His research interests are in nano electronics, nanotechnology, intelligent electronics, and intelligent sensors. Since joining KFUPM, in 2017, he has focused his efforts towards establishing a research program on Intelligent Electronics (next-generation hardware technologies for energy-efficient machine intelligence) and their use in novel applications, such as Intelligent Sensing. He was a recipient of the Australian Postgraduate Award and the National ICT Australia Ph.D. Top-Up Scholarship, from 2011 to 2015. He also received numerous prestigious regional awards by the IEEE, such as the IEEE Darrel Chong Award, for his volunteer leadership service during his early years as a student for a number of impactful regional contributions he made, such as his inception of the IEEE Middle East Student Branch Congress (ME-SBC), in 2009, which later developed to become the IEEE MESYP. He also received the Princess Sumaya Scholarship, from 2007 to 2011, and the Edexcel International High Achiever Award, in 2006, for topping all A-Level GCE examinees in Jordan. He is a member of the Australian Nanotechnology Network.